Journal of Advanced Research 62 (2024) 257–272

Contents lists available at ScienceDirect

Journal of Advanced Research

journal homepage: www.elsevier.com/locate/jare

β-Elemene induced ferroptosis via TFEB-mediated GPX4 degradation in EGFR wide-type non-small cell lung cancer

Li-Ping Zhao [1], Hao-Jie Wang [1], Die Hu, Jun-Hu Hu, Zheng-Rong Guan, Li-Hua Yu, Ya-Ping Jiang, Xiao-Qi Tang, Zhao-Huang Zhou, Tian Xie *, Jian-Shu Lou *

School of Pharmacy, Hangzhou Normal University, Hangzhou, Zhejiang 311121, China
Key Laboratory of Elemene Class Anti-Cancer Chinese Medicines Collaborative Innovation Center of Traditional Chinese Medicines of Zhejiang Province, Hangzhou Normal University, Hangzhou, Zhejiang 311121, China

GRAPHICAL ABSTRACT

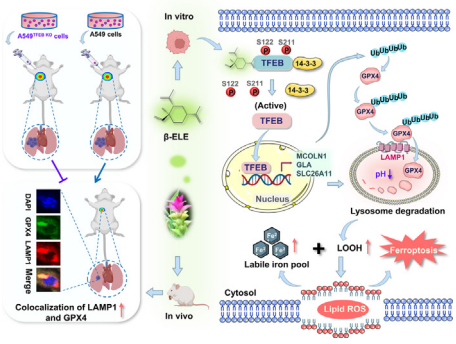

ARTICLE INFO

Article history:
Received 12 June 2023
Revised 7 August 2023
Accepted 29 August 2023
Available online 7 September 2023

Keywords:
β-Elemene
Ferroptosis
Non-small cell lung cancer
Lysosome
TFEB

ABSTRACT

Introduction: β-Elemene (β-ELE), derived from *Curcuma wenyujin*, has anticancer effect on non-small cell lung cancer (NSCLC). However, the potential target and detail mechanism were still not clear. TFEB is the master regulator of lysosome biogenesis. Ferroptosis, a promising strategy for cancer therapy could be triggered via suppression on glutathione peroxidase 4 (GPX4). Weather TFEB-mediated lysosome degradation contributes to GPX4 decline and how β-ELE modulates on this process are not clear.
Objectives: To observe the action of β-ELE on TFEB, and the role of TFEB-mediated GPX4 degradation in β-ELE induced ferroptosis.
Methods: Surface plasmon resonance (SPR) and molecular docking were applied to observe the binding affinity of β-ELE on TFEB. Activation of TFEB and lysosome were observed by immunofluorescence, western blot, flow cytometry and qPCR. Ferroptosis induced by β-ELE was observed via lipid ROS, a labile iron pool (LIP) assay and western blot. $A549^{TFEB\ KO}$ cells were established via CRISPR/Cas9. The regulation of TFEB on GPX4 and ferroptosis was observed in β-ELE treated $A549^{WT}$ and $A549^{TFEB\ KO}$ cells, which was further studied in orthotopic NOD/SCID mouse model.
Results: β-ELE can bind to TFEB, notably activate TFEB, lysosome and transcriptional increase on downstream gene GLA, MCOLN1, SLC26A11 involved in lysosome activity in EGFR wild-type NSCLC cells.

Abbreviations: β-ELE, β-Elemene; GPX4, glutathione peroxidase 4; SPR, surface plasmon resonance; NSCLC, non-small-cell lung cancer; ROS, reactive oxygen species; LIP, labile iron pool; IP, immunoprecipitation; SLC7A11, solute carrier family 7 member 11; sgRNA, single guide RNA; CA-AM, calcein acetoxymethyl ester; DFP, deferiprone; GFP, green fluorescent protein; SP, streptavidin-peroxidase; PCNA, proliferating cell nuclear antigen; MFI, mean fluorescence intensity; $TFEB^{S122A,\ S211A}$, serine-to-alanine mutation at S122 and S211 of TFEB; CMA, chaperone mediated autophagy.

* Corresponding authors.
E-mail addresses: tianxie@hznu.edu.cn (T. Xie), jlouab@connect.ust.hk (J.-S. Lou).
[1] These authors contributed equally to this work.

https://doi.org/10.1016/j.jare.2023.08.018

β-ELE increased GPX4 ubiquitination and lysosomal localization, with the increase on lysosome degradation of GPX4. Furthermore, β-ELE induced ferroptosis, which could be promoted by TFEB overexpression or compromised by TFEB knockout. Genetic knockout or inactivation of TFEB compromised β-ELE induced lysosome degradation of GPX4, which was further demonstrated in orthotopic NSCLC NOD/SCID mice model.

Conclusion: This study firstly demonstrated that TFEB promoted GPX4 lysosome degradation contributes to β-ELE induced ferroptosis in EGFR wild-type NSCLC, which gives a clue that TFEB mediated GPX4 degradation would be a novel strategy for ferroptosis induction and NSCLC therapy.

Introduction

Lung cancer is the most lethal tumor in the world and the incidence of lung cancer ranks first among all tumors in China [1]. So far, the five-year survival rate of lung cancer is <19%, and the mortality rate has not decreased. There is still no effective long-term treatment. Among the types of lung cancer, NSCLC accounts for more than 80%. Most of the patients with symptoms were found to be in the advanced stage. About 18% of the advanced patients could receive surgical treatment, and most of the remaining patients still needed drug treatment [2]. Although, EGFR-targeted therapy ushered in a new era of NSCLC therapy, the key shortages low response rate and drug resistance compromise the clinical efficacy [3]. Patients with EGFR-mutant will gain substantial benefits, while that with EGFR wild-type cannot gain any benefit, which accounts for 75%-80% of NSCLC cases [4,5]. In addition, resistance and inferior survival at the early stage is a major barrier for patients with EGFR wild-type of NSCLC [6,7]. Thus, to find promising therapeutic strategy for EGFR wild-type NSCLC patients is necessary. Interference on several biological processes could improve the efficacy of NSCLC therapy, including autophagy, ferroptosis etc. Recently, much attention has been focused on ferroptosis, which serves as a regulated cell death, driven by iron-dependent lipid peroxidation [8].

Since the discovery of ferroptosis a decade ago, numerous studies have illustrated the positive role of ferroptosis on anticancer. Induction of ferroptosis in tumor cells and immune cells can suppress tumorigenesis and progression [9,10]. Conversely, the ferroptosis evasion could facilitate cancer development and metastasis [11]. The physiology of cancer cells relies on iron. Cancer cells are more additive to iron, with high load of iron and ROS, thus, they acquire a vulnerability to the enhancement of iron and lipid peroxidation, which is prone to ferroptosis [11,12]. Therefore, targeting ferroptosis is a promising strategy for the treatment of NSCLC.

As phospholipid peroxidase GPX4 serves as the most powerful defense against ferroptosis, suppression on GPX4 attracted considerable attention for triggering ferroptosis [11]. GPX4 is a selenoprotein with its unique function on disrupting the lipid peroxidation chain reaction via suppressing of complex hydroperoxides [13]. The inhibition of GPX4 via small molecules RSL3 and erastin leads to robust increase on lipid peroxidation and consequent ferroptosis [14,15]. GPX4 can be ubiquitinated and degraded to trigger ferroptosis [16,17]. Ubiquitination of targeted proteins serve as molecular signals transferring these proteins to lysosome for degradation [18]. TFEB is the master regulator of lysosome, which activate lysosome via promoting transcription of genes involved in lysosome biogenesis. Recently, TFEB is considered as a hub of network of signals which render it as a druggable target for cancer therapy. The activation of TFEB induced by anticancer drug might contribute to lysosome mediated degradation on ferroptosis negative regulator, such as ferritin, consequently triggers ferroptosis [19]. Although the CMA mediated degradation of GPX4 has been reported recently [20,21], the regulation of TFEB on GPX4 ubiquitination and lysosome degradation has not yet been elucidated.

Different from the development of targeted therapeutic drugs, the development of some natural products was not based on their effects on specific targeted proteins, but on their promising anticancer effect and low toxicity. Many natural products have been proven to inhibit NSCLC without EGFR mutation. For instance, ginkgetin has promising effect on EGFR wild-type NSCLC [22]. Shikonin and *Marsdenia tenacissima* extract enhanced the anticancer efficacy by sensitizing EGFR wild-type NSCLC cells to gefitinib therapy [23,24]. In addition, the elderly patients who have EGFR wild-type advanced NSCLC probably gain greater survival benefit from Chinese herbal medicine [25].

β-ELE, derived from *Curcuma wenyujin*, is the main component of elemene that was approved by National Medical Products Administration in China and widely used in clinic for NSCLC therapy in China [26]. Multiple studies have demonstrated the anti-lung cancer effect of β-ELE and potential signaling pathways responsible for anticancer effect [27–29]. Nanotechnology is used to improve the stability and bioavailability of β-ELE. The early version of Lipid Nanoparticles (LN) was successfully used to make Elemene liposome, which contains 85% of β-ELE and is widely used as anticancer drug in clinic in China [26]. Subsequent LN with better stability, such as Nanostructured lipid carriers (NLCs) and Solid lipid nanoparticles (SLNs) were also developed to carry β-ELE [30,31]. Recently, novel nanocarrier stanene-based nanosheets were reported to carry β-ELE to improve its targetable and anticancer activity [32]. However, the targets for β-ELE are not fully illustrated, especially based on ligand-protein binding assay. Elucidation the mechanism induced by naturally derived anticancer drug will discover novel molecular event that contribute to anticancer effect, which will provide an effective therapeutic strategy for NSCLC. For instance, the discovery and application of topoisomerase I inhibitors as anticancer drugs is due to the mechanical study on natural product camptothecin derived from Chinese tree, *Camptotheca acuminata*. The elucidation of microtube as anticancer target of taxol, a natural compound original derived from the yew tree, Taxus brevifolia, opening a new era in the use of microtube inhibitors for anticancer [33]. Thus, the identification of target and process that can be targeted by β-ELE will give glues on novel effective anticancer approaches. Recently, it was reported that β-ELE could induce ferroptosis in lung cancer [34]. Based on "gold" standard measurement for protein-ligand binding, surface plasmon resonance (SPR), we have found β-ELE has binding affinity to TFEB. The upstream regulation of TFEB on GPX4 degradation and consequent event ferroptosis is still in its infancy. The natural compound β-ELE both have effect on TFEB and ferroptosis, using β-ELE to study the impact of TFEB on GPX4 degradation and ferroptosis will help to elucidate the unclear process of TFEB-mediated GPX4 lysosome degradation, which could be developed to be a novel strategy for ferroptosis induction and anti-NSCLC therapy.

Materials and methods

Reagents and antibodies

β-ELE was obtained from LKT Labs Co., Ltd (St. Paul, MN, USA, purity ≥ 98%). β-ELE was dissolved in absolute ethanol (E7148, Merck, USA, purity ≥ 99.5%) and diluted to the desired concentration. The antibodies were used as following, GAPDH (60004–1, Proteintech), PCNA (2586, Cell Signaling Technology), solute carrier family 7 member 11 (SLC7A11) (12691, Cell Signaling Technology), Phospho-TFEB (Ser122) (86843, Cell Signaling Technology), Lamin B1 (13435, Cell Signaling Technology), Ubiquitin (P4D1) (3936, Cell Signaling Technology), FTH (4393, Cell Signaling Technology), Phospho-TFEB (Ser211) (37681, Cell Signaling Technology), 14–3-3 (8312, Cell Signaling Technology), GPX4 (ab125066, Abcam), LAMP1 (sc-20011, Santa Cruz Biotechnology), TFEB (ab267351, Abcam), Ferritin (ab75973, Abcam).

SPR assay

SPR assay was performed in a GE Life Sciences Biacore S200 with a GE series S CM5 sensor chip. Briefly, TFEB (OriGene, MD, USA) were covalently immobilized onto the chip surface through their amine groups. The immobilization level of the protein was around 4200 RU. Different concentrations of β-ELE (2-fold dilutions from 50 μM to 3.125 μM) were flown through the chip surface, and their interactions with TFEB were monitored in real time. A reference channel with no fixed protein and compound-free solution was used to subtract any non-specific signal. The whole system was run under 10 mM HEPES, pH 7.4, 150 mM NaCl, 0.05% P20, 2% DMSO with a controlled temperature of 25 °C. Data was analyzed using GE Biacore S200 control software.

Molecular docking

AutoDock Vina (Vina, version 1.1.2) was used as the molecular docking program in this study. It can operate with a semi-flexible docking method with a docking accuracy of 78%. The 3D structure of β-ELE (CID: 6918391) was retrieved from the chemical database of PubChem. The 3D structure of protein TFEB was kindly provided by Dr. Pengfei Fang (University of Chinese Academy of Sciences). TFEB protein was assigned as the receptor and β-ELE as the ligand. The docking calculations were performed using the AutoDock Vina version 4.2 (ADT4.2). Protein and ligand were loaded in ADT. The receptor protein was solvated with water, and only polar hydrogens were added. The receptor grid boxes (in X, Y, Z dimension) were established in ADT4.2, and the pdbqt files of proteins were generated. The protein-ligand complex was visualized and analyzed by PyMOL software (The PyMOL Molecular Graphics System, Version 4.3.0 Schrödinger, LLC, San Diego, CA, USA).

Cell culture

A549 cells were obtained from the American Type Culture Collection (ATCC, USA). The NCI-H460 and SPC-A-1 cells were obtained from the Cell Bank of the Chinese Academy of Sciences (Shanghai, China). Roswell Park Memorial Institute (RPMI) 1640 (Gibco, Thermo Fisher Scientific, Inc.) with 10% FBS (Gibco, Thermo Fisher Scientific, Inc.), 100 U/mL penicillin and 100 mg/L streptomycin (HyClone, USA) was used to culture NSCLC cells in a 5% CO_2 at 37 °C. The medium was changed every 1 or 2 days and the NSCLC cells were expanded until passage ten (in the logarithmic phase) after thawing and then utilized in further studies.

Establishment of TFEB knockout cells

$A549^{TFEB\ KO}$ cells were established through the CRISPR/Cas9 genome editing system. The $TFEB^{KO}$-based CRISPR plasmid were designed and generated by WZ Biosciences (Shandong, China). The single guide RNA (sgRNA) sequence was 5′-GCGGGAGCGCATG CAGCAAC-3′ to disrupt the TFEB gene. To produce lentiviruses, 7×10^5 HEK 293 T cells were plated in 6 cm culture dish and were transfected the next day with 6 μg CRISPR plasmid, 5 μg psPAX2, and 2.5 μg pMD2.G using Lipo3000 transfection reagent (L3000015, Invitrogen) according to the manufacturer's instructions. After 8 h, removed the medium containing transfection reagent and added fresh medium. The supernatant suspensions were harvested 48 h after transfection, and stored at -80 °C. To construct knockout cells, A549 cells were seeded into a 6-well plate at a density of 5×10^5 cells, and subsequently infected with the $TFEB^{KO}$ plasmid-encoding lentivirus for entire two days. Then A549 cells were selected in a culture medium with 20 μg/mL puromycin (Biosharp, China) for 2 weeks, and western blot technology was used to identify whether the gene was knocked out.

Western blot analysis

Treated cells or fresh tissues were washed twice with ice-cold PBS (pH 7.4) and lysed in the RIPA buffer containing 100 mM HEPES, 150 mM NaCl, 1 mM EGTA, 1 mM EDTA, 1% Triton, 1% NP-40, 3 mM benzamidine, 10 mM NaF, 1 mM Na_3VO_4, 10 μg/mL aprotinin and 10 μg/mL leupeptin (pH 7.5). The collected cell lysates were incubated on ice and vortexed for three times, 5 min/-time. Cell lysates were centrifuged (12,000 × g) for 30 min at 4 °C. Protein concentration in whole-cell lysates was quantified by BCA Assay with BCA Protein Assay Kit (ThermoFisher, USA). The cell lysates were boiled in a sample loading buffer (10% glycerol, 5% β-mercaptoethanol, 2% SDS, 50 mM Tris-HCl, pH 6.8, 0.05% bromophenol blue) at 95 °C for 10 min. Separation gels and stacking gels were fabricated. In total, 20 to 60 μg of proteins were separated on 4-20% sodium dodecyl sulfate (SDS)-polyacrylamide gel electrophoresis (PAGE) and transferred to polyvinylidene difluoride (PVDF) membrane (Millipore, Bedford, MA, USA). Then it was blocked with 5% nonfat milk in TBST for 1 h at room temperature and then incubated with primary antibody overnight at 4 °C. Next day, incubated the membrane with the secondary antibody (Cell Signaling Technology, USA) for 1 h at 24 °C. The immunoreactivity signals were developed after adding ECL reagent (Beyotime, Shanghai, China) and recorded by a ChemiDoc Imaging System (Bio-Rad, USA). The gray levels of protein bands were obtained by Image Lab software (Bio-Rad, USA).

RNA isolation and quantitative real-time PCR

Total RNA was extracted by RNA-easy Isolation Reagent (R701-01/02, Vazyme, China) . After quantification by a NanoDrop 2000 (Thermo, USA). cDNA synthesis was carried out using Hiscript III Reverse Transcriptase (R302-01, Vazyme, China) according to the manufacturer's protocols. qPCR was performed using synthesized primers (Tsingke Biological Technology, China) and SYBR green master mix (Q121-02, Vazyme, China). The relative mRNA expressions were analyzed based on the $2^{-\Delta\Delta CT}$ method. ACTB was used as a reference gene for mRNA. The total reaction volume was 10 μL. The amplification program included activation of the enzyme at 95 °C for 30 s, followed by 40 cycles of denaturation at 95 °C for 15 s, annealing and extension at 60 °C for 30 s, and 72 °C for 30 s.

The following primers were used: 5′-AAAGCCTTCGCATCTCA GAATAA' (S) and 5′-GGCAGACTTGGGGATGTAGTA' (AS) for SLC26A11; 5′-GCCTTCCGAC ACCTCTTCC' (S) and 5′-CCACGGA CAT-

ACGCATACCG' (AS) for MCOLN1; 5′-TTGGATACTACGACATT GATGCC' (S) and 5′-TTCTGCCAGTCCTATTCAGG G' (AS) for GLA; 5′-GAGGCAAGACCGAAGTAAACTAC' (S) and 5′-CCGAACT GGTTA-CACGGGAA' (AS) for GPX4; 5′-CATGTACGTTGCTATCCAGGC' (S) and 5′-CTCCTTAATGTCACGCACGAT' (AS) for ACTB.

Cytotoxicity assay

Cells (3×10^3/well) were seeded in 96-well plates. After fully adhered to the plate, the medium was replaced, and the cells were treated with β-ELE (120 μg/mL) for 24 h. For CCK8 assay, added 20 μL CCK8 solution (Solarbio, Beijing, China), the absorbance was measured at 450 nm after 4 h incubation. For MTT assay, added 20 μL MTT solution into each well (5 mg/mL, Sigma Aldrich). Remove the liquid after incubation at dark. Add 150 μL DMSO to each well and shake the plate for 15 min to facilitate dissolution of the crystals. Measured the absorbance at 570 nm by an microplate reader (Thermo Fisher Scientific, USA). The OD value of treated cells relative to that of the untreated cells was expressed as a percentage of cellular viability.

Lipid ROS assay

NSCLC cells were seeded in 6 cm culture dishes and incubated for 12 h to allow cells to reach the exponential growth phase, then treated or untreated with β-ELE (120 μg/mL) for 24 h. Fresh medium containing 10 μM BODIPY 581/591 C11 (D3861, Invitrogen) was added to each well for lipid peroxidation measurements. After incubation for 30 min at 37 °C, 5% CO_2, discard the medium and the cells were washed with PBS twise. Cells were resuspended in 1 ml PBS with the density of 0.5×10^6 cells/mL. Cell suspension were transferred to Falcon 5 ml 12 × 75 mm polystyrene round-bottom tubes (BD Falcon cat. number 352054). Fluorescence intensity of 10,000 cells per sample was measured by flow cytometry (Exc = 488 nm, Em = 510) (BD Bioscience, USA), and the results were analyzed with Flowjo v10 software.

Lysosome acidification measurement

LysoTracker™ Red DND-99 (L7528, Thermo Fisher Scientific) is a red-fluorescent dye for labeling and tracking acidic organelles in live cells, and the intra-lysosomal pH was estimated by using it. After NSCLC cells treated or untreated with β-ELE (120 μg/mL) for 24 h, fresh medium containing 50 nM LysoTracker™ Red DND-99 was added to each well for lysosome acidification measurement. Cells were washed in PBS, then added 4% paraformaldehyde (PFA) (Sangon Biotech, China) at 4 °C for 10 min, and then washed with PBS. Nuclei were stained with DAPI for 5 min. Cells were washed with TBS and observed under the fluorescence microscope (Olympus FLUOVIEW FV3000). For live-cell Lyso-Tracker flow cytometry analysis, cells were seeded in 6 cm dishes and treated with or without β-ELE (120 μg/mL) for 24 h after cells have grown to about 70% confluence. After 24 h, cells were treated with 50 nM Lyso-Tracker Red DND-99 for 30 min. After washing twice with PBS, added trypsinization with 0.05% trypsin EDTA (HyClone, USA). After washing with PBS, cells were analyzed by flow cytometry (BD Bioscience, USA) at 561 nm excitation.

Immunofluorescence staining and confocal microscopic observation

A549 cells were plated on coverslips. Cells were treated with or without β-ELE (120 μg/mL) for 24 h. The coverslips were washed with PBS and fixed in 4% PFA (Sangon Biotech, China) for 15 min at room temperature, then blocked (1 × PBS/5% BSA/0.3% Triton™ X-100) for 1 h. Subsequently, cells were incubated with anti-GPX4 (1:250) and anti-LAMP1 (1:250) antibodies at 4 °C overnight and then incubated with Alexa Fluor 546-conjugated goat anti-mouse secondary or Alexa Fluor 488-conjugated goat anti-rabbit together with DAPI for 1 h at room temperature. After washing three times with PBS, the stained cells were mounted by using an anti-fade mounting medium (S2100, SolarBio, Beijing, China), and images were captured by using a confocal laser-scanning microscope (Olympus FLUOVIEW FV3000). The co-localization coefficients were observed by Olympus Fluoview FV31S-DT Software.

LIP assay

Upon entering viable cells, calcein acetoxymethyl ester (CA-AM, YEASEN) undergoes hydrolysis by esterases to calcein (CA) and becomes fluorescent. Its fluorescence is quenched upon binding to cellular LIP, in a stochiometric fashion. The addition of a high-affinity chelator, such as deferiprone (DFP, MedChemExpress), which removes iron from its complex with CA, increases the fluorescence emitted by the cells. Cells (3×10^5/well) grew in 6 cm dishes. β-ELE (120 μg/mL) treated and untreated cells were collected and then washed with PBS twice. Incubated cells with 0.5 μM CA-AM for 15 min at 37 °C. Washed cells with PBS and added iron chelator DFP at 100 μM or left untreated. Cells were collected and analyzed by flow cytometry (BD Bioscience, USA) (excitation 488 nm, emission 517 nm). Cells were analyzed with the FlowJo software (USA). Mean fluorescence intensity (MFI) increases with decreasing free iron content. The magnitude of iron chelation is calculated as ΔMFI (MFI CA-AM/DFP – MFI CA-AM alone) before and after treatment with β-ELE (120 μg/mL) as previously described.

Immunoprecipitation (IP)

A549 cells were transfected with the indicated plasmids (GPX4 or TFEB) by using Lipo3000 transfection reagent (L3000015, Invitrogen). After treated with β-ELE (120 μg/mL) for 24 h, cells were harvested and lysed with IP lysis buffer (1% NP-40, 150 mM NaCl, 25 mM Tris pH 7.4, 0.5% sodium deoxycholate, 0.1% SDS) containing a cocktail of protease inhibitors (Roche). One milligram of total protein in 500 μL cooled IP buffer (1% NP-40, 150 mM NaCl, 25 mM Tris pH 7.4, 0.5% sodium deoxycholate, 0.1% SDS and protease inhibitor cocktail) was incubated with 20 μL anti-green fluorescent protein (GFP) nanobeads, and they were slowly shaken on a rotator at 4 °C overnight. After centrifugation 300 × g for 5 min, washed the pellet three times with lysis buffer, and the beads were boiled in 2 × sample loading buffer for western blot.

GFP nano-beads preparation

DNA encoding anti-GFP nanobody with His-tag was expressed in *E. coli* BL21 cells. Cells were grown at 37 °C with shaking (250 rpm), 0.5 mM isopropyl-β-D-1-thiogalactopyranoside (IPTG) was added when OD value reached 0.6–0.8, then shaking at 18 °C. Cells were harvested after 16 h by centrifugation at 4000 × rpm for 20 min. Cell pellets were suspended in 50 ml wash buffer (20 mM HEPES (CAS:7365–45-9, MW:238.31), 15 mM NaCl, PH 7.0) containing 500 μL phenylmethylsulfonyl fluoride (PMSF, 1 mM) and lysed using a High Pressure Homogenizer (JN-02C, JNBIO, China) at 1,000 bar for 5 times. The cell debris were removed by centrifugation at 35000 × g for 30 min. The supernatant was applied to a Ni-NTA (Qiagen) column pre-equilibrated with 30 mM imidazole. The mixture was rotated at 4 °C for 1 h, the beads were washed to remove unbound protein with wash buffer. Anti-GFP nanobody was eluted sequentially with low (30 mM) and high (500 mM) concentrations of imidazole in buffer (20 mM

HEPES, 150 mM NaCl, PH 7.0), and concentrated with 100 kDa molecular weight cut-off concentrators (Milipore).

Incubate a ratio of 1 mg:100 μL anti-GFP nanobody solution to NHS-activated agarose slurry (GE Healthcare) at 4 °C to couple the anti-GFP nanobody to the resin overnight. Then the resin was washed with 10 column volumes of blocking buffer (0.1 M Tris-HCl pH 8.0) to remove unbound nanobody, followed by incubation at 25 °C for 2 h to quench unreacted NHS sites. Once blocking was complete, washed the resin six times with wash buffer (bufer 1: 0.1 M Tris-HCl pH 8.0, 0.5 M NaCl, and bufer 2: 0.1 M sodium acetate, 0.5 M NaCl, pH 4.0). GFP nano-beads and the interaction with target protein were measured by IP assay. Anti-GFP resin was stored in storage buffer (10 mM Tris-HCl pH 8.0, 150 mM NaCl) and stored at 4 °C.

Animal experiments

A549 and A549$^{TFEB\ KO}$ cells were retrovirally infected with a fusion protein reporter construct encoding GFP and firefly luciferase. Then cells stably expressing the luciferase reporter gene were screened with puromycin. 4-5 week-old male NOD/SCID mice (18-20 g) were obtained from Shanghai SLAC Laboratory Animal Co., Ltd (Shanghai, China). Mice were anesthetized with 1.25% tribromoethanol (125 mg/kg) and placed in the left lateral decubitus position.

Carefully made a small incision (3-5 mm) in the right chest area by using surgical scissors, and then remove soft tissue to expose the sternocostal and intercostal spaces. The injection site was determined by a marker (between the fifth and sixth ribs, the right anterior axillary line). A549-luci or A549 $^{TFEB\ KO}$-luci cells (1×10^6) were injected into the right lung. After tumor injection, observed the mice for 45 to 60 min until they were fully recovered. Five days later, miece were divided into 4 groups (one group of six) and treated withvehicle or β-ELE (120 mg/kg) by a tail vein injection every day. Observed the tumor size of each mouse every week. Briefly, mice were intraperitoneal injected of 50 μL luciferin solution (30 mg/mL stock) per 10 g prior to isoflurane anesthesia, and fluorescence radiance was detected by Biospace Lab Photon Imager Optima (Nesles-la-Valee, France). Biospace Lab Photon Imager Optima was equipped with a highly sensitive cooled CCD camera. The mouse was anesthetized using an isoflurane chamber and then positioned inside the imager (ventral side up for the orthotopic models), with its nose in an isoflurane nosecone to maintain anaesthesia. After image acquisition, routinely performed for 1 min, mouse was placed back in its cage. The time profile of the signal acquisition ensures that the signal was acquired while the luciferin is in the saturation state. The data were analyzed with M3 Vision™ software provided by Biospace. On day 21 after administration, mice were sacrificed and tumor tissue samples were frozen in -80 °C or fixed in 4% PFA for IF or IHC respectively.

Immunohistochemistry

Tumor samples were fixed with 4% PFA in PBS, snap-frozen in OCT compound and serially sectioned at a thickness of 6 μm. IHC was carried out to visualize cells by using proliferating cell nuclear antigen (PCNA) antibody. Six field images were collected by using a fluorescence microscope (DS-Ri1, Nikon, Japan). The IOD index of PCNA was analyzed by Image Pro Plus software.

Ethics statement

All animal experiments were performed in accordance with the National Research Council Guidelines for Laboratory Care and Use and approved by the Experimental Animal Ethics Committee of Hangzhou Normal University. (Approval number: 2021–1123).

Statistical analysis

GraphPad Prism 8.0.1 was used for statistical analysis. Data was repeated at least three independent experiments and presented as the ± standard error of mean (SEM). The significant differences between two groups and multiple groups can be determined by two-tailed t-tests and one-way analysis of variance, respectively. Statistical significance was assessed by statistics with $P < 0.05$. *, P values of < 0.05; **, $P < 0.01$; ***, $P < 0.001$.

Results

β-ELE binds to TFEB and induces TFEB activation

Our previous study found that blocking lysosome activity could reverse β-ELE induced anticancer effect. Thus, we thought it might be effected on the crucial regulator during lysosome biogenesis. TFEB is the master regulator for lysosome biogenesis, thus, we first applied SPR assay to observe if β-ELE has binding affinity to TFEB. SPR sensorgrams showed that the binding response curves exhibit in a dose-dependent manner, and the KD value is 8.296E-5 M, while the vehicle has no binding response, which indicated that β-ELE has binding affinity to TFEB (Fig. 1A, B&D). Up to now, no protein-ligand binding experiment was applied to investigate the binding proteins of β-ELE in reported studies, thus, this is the first time to find a potential targeted protein, TFEB, can bind to β-ELE. To provide deeper insight into the binding interactions between β-ELE and TFEB, a molecular docking simulation was performed by Autodock Vina. β-ELE interacts with the TFEB residues of Thr308, Asn309, Leu312, and Trp313 with average binding energy −5.0 kcal/mol, which indicated the potential of direct binding between β-ELE and TFEB (Fig. 1C). These residues are located on the ZIP region of TFEB, which was responsible for TFEB activation and nuclear translocation, thus, we observed the activation of TFEB in β-ELE treated NSCLC cells.

Dephosphorylation of TFEB at S122, S211 leading to the activation and nuclear translocation of TFEB. To observe the effect of β-ELE on TFEB activation, we firstly detected the phosphorylation levels of TFEB. β-ELE (120 μg/mL) notably decreased the phoysphorylation levels of TFEB at S122, S211, as well as its binding protein 14-3-3 (Fig. 1E&S1A), which indicated that β-ELE may promote dephosphorylation of TFEB, consequently increase its nuclear translocation and activation. To observe the nuclear translocation of endogenous TFEB in response to β-ELE treatment, subcellular fractionation and western blot were performed on A549, SPC-A-1 and NCI-H460 cells. After the treatment with β-ELE (120 μg/mL) for 12 h, 24 h, and 48 h, the protein expression of TFEB in nucleus were all significantly increased in these three cell lines (Fig. 1F&S1B). These results indicated that β-ELE induces TFEB nuclear translocation, which were further confirmed by the immunofluorescence assay on A549, SPC-A-1 and NCI-H460 cells. The fluorescence intensity of TFEB was observed both in cytosol and nucleus. In control group, the fluorescence was mainly located in cytosol, and a faint signal was observed in nucleus, as demonstrated by co-localization of DAPI signal. Application of β-ELE (120 μg/mL) for 24 h significantly increased the TFEB fluorescence intensity in nucleus (Fig. 1G). To find if the increased nuclear translocation of TFEB due to the increase on the total amount of TFEB, we detected both mRNA and protein level of TFEB. β-ELE has no obviously effect on mRNA and protein level of TFEB (Fig. S1C&1E), which indicated that the increase of nuclear translocation of TFEB is not due to the increase of TFEB. All these data

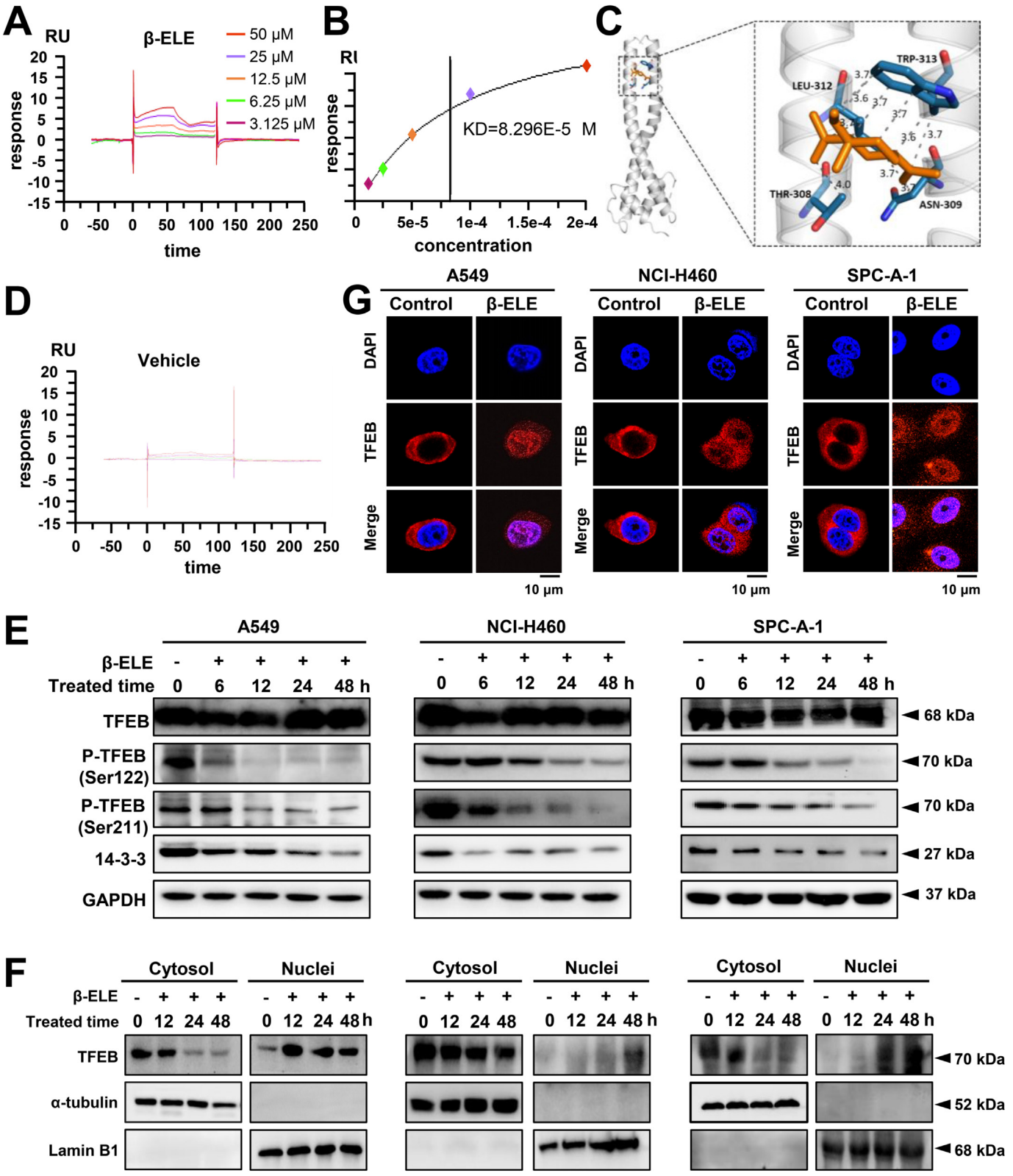

Fig. 1. β-ELE binds to TFEB and induces TFEB activation. (A) Different concentrations of β-ELE (50 μM, 25 μM, 12.5 μM, 6.25 μM, 3.125 μM) flowed over the surface of a CM5 chip immobilized with TFEB protein. Interaction profile is recorded in real-time in a sensorgram. (B) The binding curves from (A). (C) Molecular docking simulation of β-ELE to HLH-ZIP region of TFEB by the Autodock Vina program. It showed the interaction of β-ELE (shown in orange color and stick model) with active site residues of TFEB (grey). The amino acids in position 308, 309, 312, 313 forms an H-bond with β-ELE (Hydrogen bonds were represented as grey dotted lines and their distances were labeled in angstrom). (D) The sensorgram of vehicle with HLH-ZIP region of TFEB. (E) β-ELE treated on A549, NCI-H460, and SPC-A-1 cells for 6, 12, 24, and 48 h, the protein expressions of TFEB, p-TFEB (Ser122), p-TFEB (Ser211) and 14-3-3 were analyzed by western blot. (F) β-ELE treated on A549, NCI-H460, and SPC-A-1 cells for 12, 24, and 48 h, the protein expression of TFEB in nuclei and cytosol were detected by western blot. α-tubulin served as a cytoplasmic marker protein, Lamin B1 served as a nuclear marker protein. (G) β-ELE treated on A549, NCI-H460, and SPC-A-1 cells for 24 h, the localization of TFEB (red fluorescence) in nuclei (blue fluorescence) was observed by immunofluorescence. Bar = 10 μm. Data are presented as means ± SEM from three independent experiments.

indicated that β-ELE can activate TFEB on A549, SPC-A-1 and NCI-H460 NSCLC cells.

β-ELE regulates lysosomal biogenesis

TFEB can promote lysosome biogenesis, whether β-ELE induced activation on TFEB could consequently activate lysosome has not been reported. In order to examine the effect of β-ELE on lysosome, we observed the changes of lysosomal function in NSCLC cells. First, LysoTracker staining showed that the mean fluorescence intensity was sharply increased by β-ELE in A549, SPC-A-1 and NCI-H460 cells, indicating enhanced acidification of lysosome (Fig. 2A, D&G). These phenomena were confirmed by flow cytometry, a shift in fluorescence to higher intensities and the notable increase in mean fluorescence intensity (MFI) were observed in all these three NSCLC cells (Fig. 2B, E&H). Second, we observed the gene expression involved in lysosome biogenesis, including lysosomal hydrolases and accessory protein GLA, lysosomal membrane protein MCOLN1, SLC26A11. The application of β-ELE significantly increased the mRNA expression of these genes (Fig. 2C, F&I). As they are all transcriptionally regulated by TFEB, the upregulation of mRNA level may due to the activation of TFEB, consequently activate lysosome.

β-ELE promotes GPX4 lysosome degradation in NSCLC

Considering β-ELE could promote TFEB-mediated lysosome activation, and negative regulators of ferroptosis could be degraded via lysosome degradation, thus, we hypothesis that β-ELE could degrade negative regulator of ferroptosis. As the activation on TFEB and lysosome induced by β-ELE were mostly obvious on A549, we chosen this cell line for mechanism study. Here, we found β-ELE significantly decrease the key negative regulator of ferroptosis GPX4. To investigate whether the decline of GPX4 is due to the change on transcriptional or post transcriptional regulation, we firstly detected the change on mRNA level of GPX4, no obvious change was found in β-ELE treated A549 cells (Fig. 3A). Thus, the decline of GPX4 was not due to the transcription. Then, we applied proteasome inhibitor MG132 or lysosomal degradation inhibitors BafA1 and CQ in β-ELE treated A549 cells. MG132 could not significantly reversed the decline of GPX4, while both BafA1 and CQ robustly attenuated β-ELE induced decrease on GPX4 (Fig. 3B&S2A), which indicated that β-ELE might induce lysosome degradation of GPX4. As ubiquitination process is required to transfer protein to lysosome for degradation, we observed the ubiquitination of GPX4. The immunoprecipitation assay indicated that the polyubiquitination chain was increased in a time dependent manner in β-ELE treated A549 cells (Fig. 3C&S2B). Next, we purified lysosome fraction to observed the distribution of GPX4 in lysosome. β-ELE notably increased the amount of GPX4 in lysosome, while that is decreased in lysosome free fraction (Fig. 3E&S2C), which was further confirmed by immunostaining assay, the co-localization of GPX4 and LAMP1 was about two fold increase after the treatment of β-ELE (Fig. 3D&F). All these data indicated that β-ELE promoted GPX4 lysosome degradation. The mechanical studies of β-ELE are seldom focus on lysosome degradation, thus, this result provided a new perspective on the mechanism of β-ELE induced anticancer effect, and pave us to find out the relationship of its binding protein TFEB and GPX4 lysosome degradation.

TFEB promotes GPX4 lysosome degradation in β-ELE treated NSCLC

β-ELE promoted lysosome degradation of GPX4, considering β-ELE induced lysosome activation was positively related to TFEB, thus, TFEB might be the upstream regulator for GPX4 reduction in β-ELE treated NSCLC cells. The role of TFEB on GPX4 degradation has not been illustrated, this might be a novel biological event during anticancer process triggered by anticancer agents, such like β-ELE. In order to observe the role of TFEB in β-ELE induced lysosome degradation, we established TFEB knockout A549 cell line A549$^{TFEB\ KO}$ (Fig. S3A).To further confirm this, we applied β-ELE on either A549 or A549$^{TFEB\ KO}$ cells. The result indicated that the reduced level of GPX4 induced by β-ELE was notable reversed in A549$^{TFEB\ KO}$ cells, and the overexpression of TFEB restored the decrease on GPX4 (Fig. 4A&S3B). Dephosphorylation of TFEB could increase its activity and vice versa. Next, we generated a plasmid with serine-to-alanine mutation at S122 and S211 of TFEB (TFEB$^{S122A,\ S211A}$) to mimic the dephosphorylation of TFEB, as well as the plasmids with mutation on S122, S211 or double mutation on S122 and S211(TFEB^{S122D}, TFEB^{S211D}, and TFEB$^{S122D,\ S211D}$) to mimic the phosphorylation of TFEB. β-ELE induced decrease of GPX4 was significantly promoted in TFEB$^{S122A,\ S211A}$ transfected A549 cells (Fig. 4B&S3C). On the contrary, the decrease of GPX4 was notably reversed when A549 cells transfected with TFEB$^{S122D,\ S211D}$ (Fig. 4B&S3C). These results further demonstrated that TFEB promoted GPX4 decline in β-ELE treated NSCLC cells. To investigate whether the ubiquitination of GPX4 induced by β-ELE is related to TFEB, we co-transfected TFEB and GPX4 on A549 cells, and observed the changes of ubiquitin chains bound to GPX4 by immunoprecipitation. At the same time, we also transfected GPX4 on A549$^{TFEB\ KO}$ cells. The results showed that after the treatment of β-ELE, the ubiquitin chains bound to GPX4 were significantly increased compared with GPX4 single-transfection (Fig. 4C&S3D), while the ubiquitin chains bound to GPX4 were decreased in A549$^{TFEB\ KO}$ cells compared with that in A549 cells (Fig. 4D&S3E). We further compared the content of GPX4 in lysosomes with β-ELE applied on either A549 or A549$^{TFEB\ KO}$ cells. Our results showed that knockout of TFEB decrease lysosomal GPX4 (Fig. 4F&S3F). Through immunofluorescence experiments, it was found that the green fluorescence of GPX4 in A549 cells decreased after β-ELE treatment, while the red fluorescence of LAMP1 increased, indicating that β-ELE treatment reduced the expression of GPX4 and activated lysosomes. At the same time, the co-localization of GPX4 and LAMP1 increased, indicating that β-ELE promoted the lysosomal distribution of GPX4 (Fig. 4E). In order to further prove the effect of TFEB on the distribution of GPX4 in lysosomes, we administered β-ELE to A549$^{TFEB\ KO}$ cells, and found that the fluorescence intensity of GPX4 was enhanced compared with A549 cells administered with β-ELE, the red fluorescence of LAMP1 was weakened, indicating that β-ELE-induced GPX4 degradation and lysosome activation were inhibited after TFEB knockout. Meantime, β-ELE induced increase on the co-localization of LAMP1 and GPX4 was attenuated in A549$^{TFEB\ KO}$ cells (Fig. 4E&G). These phenomena indicated that TFEB knockout may reduce the lysosomal degradation of GPX4 by reducing its lysosomal distribution, thereby inhibiting the reduction of GPX4 in β-ELE treated A549 cells.

β-ELE induces ferroptosis in NSCLC

The reduction of GPX4 could induce ferroptosis. As either directly or indirectly ferroptosis induction need downregulation on GPX4, it was the key negative regulator involved in ferroptosis. The two key features for ferroptosis are the increase on lipid ROS and intracellular iron. To evaluate the effect of β-ELE on ferroptosis induction in NSCLC cells. We firstly observed the lipid ROS and liable iron pool in β-ELE treated NSCLC cells. β-ELE significantly increased the lipid ROS (Fig. 5A&B), as well as liable iron pool in A549 (Fig. 5C&D). The similar phenomenon was also found in NCI-H460 (Fig. S5A,B,C&D) and SPC-A-1 cells (Fig. S6A,B,C&D), however the increase on liable iron pool was not as obvious as that

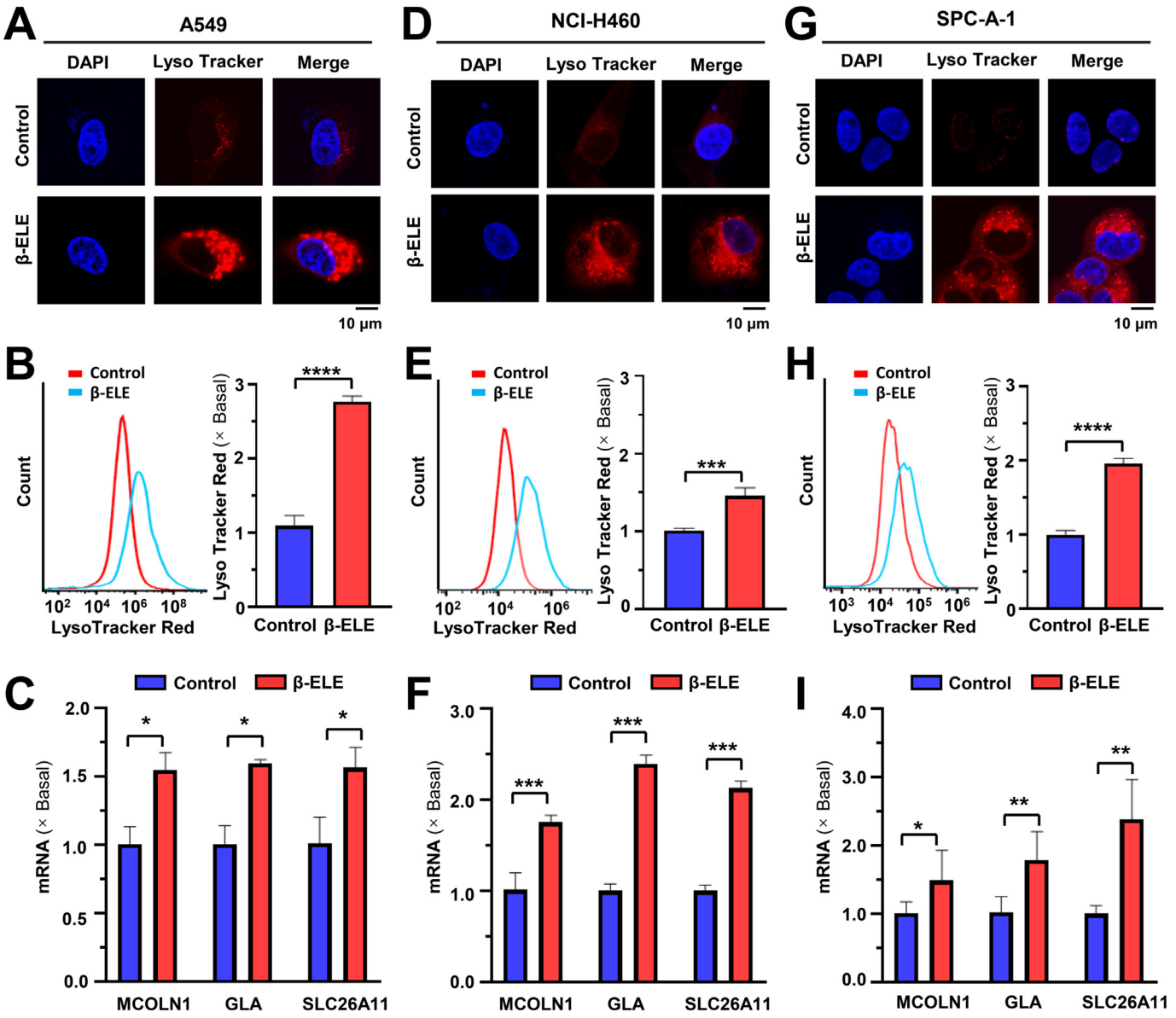

Fig. 2. β-ELE promotes lysosomal biogenesis. (A, D, G) β-ELE treated on A549 (A), NCI-H460 (D), and SPC-A-1 (G) cells for 24 h. The fluorescent signals were detected by confocal microscopy after staining with LysoTracker Red (50 nM) for 30 min. Bar = 10 μm. (B, E, H) β-ELE treated on A549 (B), NCI-H460 (E), and SPC-A-1(H) cells for 24 h. Cells were then loaded with LysoTracker Red (50 nM) for 30 min. Fluorescence intensity of 10,000 cells per sample was measured by flow cytometry. (C, F, I) β-ELE treated on A549 (C), NCI-H460 (F), and SPC-A-1 (I) cells for 24 h, the amount of mRNA encoding MCOLN1, SLC26A11, and GLA were determined by real-time PCR. mRNA was normalized with ACTB. $n = 3$, $^{*}P < 0.05$, $^{**}P < 0.01$, $^{***}P < 0.001$.

in A549, which was accordance with the change on TFEB and lysosome activation. Next, we observed the key factors involved in ferroptosis. The application of β-ELE time-dependently decreased the expression of GPX4, significantly decrease were observed on 12 h, 24 h, 48 h, while the obvious decline on ferritin and FTH were only observed on 48 h, and the notable changes on SLC7A11 were not found in A549 (Fig. 5E&S4). This phenomena were also found in NCI-H460 (Fig. S5E&G) and SPC-A-1 cells (Fig. S6E&G), however, the decreases on GPX4 were also less obvious than that in A549. The robust decrease of GPX4 in all these three cell lines indicated that GPX4 decline may contribute to β-ELE mediated ferroptosis. To further confirm the ferroptosis induction induced by β-ELE, we applied two ferroptosis inhibitors ferrostatin-1 and liproxstatin-1 to investigate the change on β-ELE induced cytotoxicity on NSCLC cells. The decreases in cell viability induced by β-ELE were sharply attenuated by ferroptosis inhibitors in all these three cell lines, and this phenomenon was mostly obvious in A549 cell line (Fig. 5F, S5F&S6F). β-ELE could promote targeted therapeutic drugs via ferroptosis induction in EGFR-mutant NSCLC [35], however, its single role on ferroptosis in EGFR wide type NSCLC has not been illustrated. These data indicated that β-ELE can induce ferroptosis in NSCLC cells, and the phenomenon was most obviously in A549, as well as the activation of TFEB and lysosome.

TFEB promotes β-ELE induced ferroptosis in NSCLC

Both GPX4 reduction and ferroptosis induction could induced by β-ELE, and GPX4 lysosome reduction was positively related to TFEB, thus, TFEB might be the upstream regulator on β-ELE induced ferroptosis. Here, we found β-ELE induced cytotoxicity and lipid ROS enhancement were obviously reversed by TFEB knockout

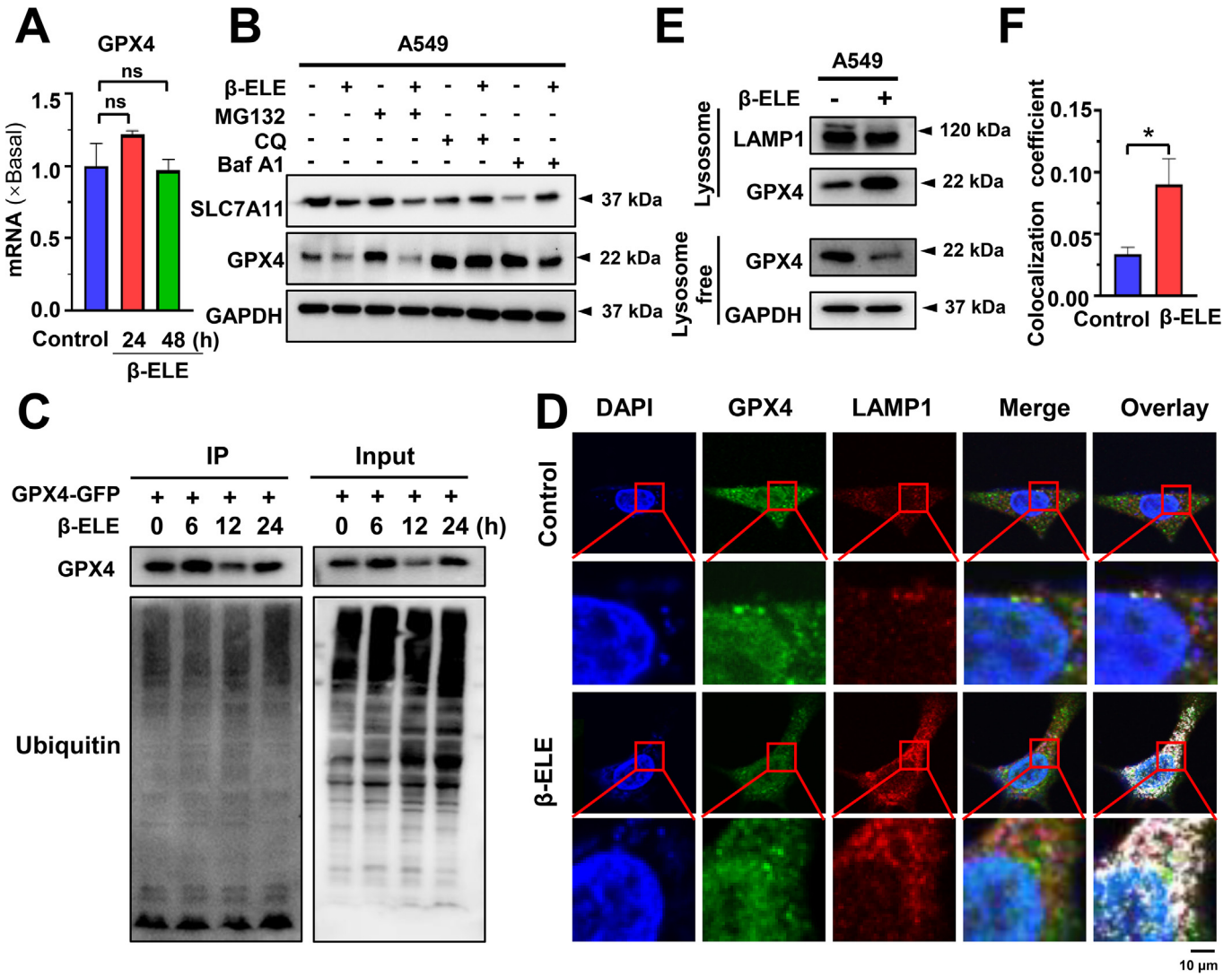

Fig. 3. β-ELE promoted GPX4 degradation in NSCLC cells. (A) Quantification of GPX4 mRNA levels by qPCR in A549 cells treated with β-ELE (120 μg/mL) for different time points (24, 48 h). mRNA was normalized with ACTB, and "ns" means no statistical difference. (B) A549 cells were treated with β-ELE (120 μg/mL) after with or without the pretreatment of proteasome inhibitor MG132 (1 μM) or lysosomal degradation inhibitor BafA1 (160 nM)、CQ (20 μM) for 1 h. The changes of SLC7A11 and GPX4 protein levels were detected by western blot. (C) A549 cells were transfected with GPX4-GFP (10 μg/10 cm dish), then treated with β-ELE (120 μg/mL) for 6, 12, and 24 h. Cells were harvested and lysed with RIPA buffer, cell lysates were then subjected to immunoprecipitation (IP) via GFP-nanobeads and analyzed by western blotting with antibodies as indicated (GPX4, ubiquitin). (D) β-ELE (120 μg/mL) treated on A549 cells for 24 h, the co-localization of LAMP1 and GPX4 was detected by immunofluorescence. A green fluorescent signal representing GPX4 was distributed in both the cytoplasm and nucleus, and the red fluorescent signal representing LAMP1 was mainly distributed in the cytoplasm. Bar = 10 μm. (E) A549 cells were treated with β-ELE (120 μg/mL) for 24 h. Lysosomes and lysosome-free cell lysates were collected, the protein level of GPX4 was measured by western blot. LAMP1 and GAPDH were used as loading controls of lysosomal and non-lysosomal fractions, respectively. (F) Co-localization coefficients in (D) were calculated by Olympus Fluoview FV31S-DT Software. Each point represents the mean ± SEM, $n = 4$, $^{*}P < 0.05$.

(Fig. 6A&B). The reversed effect on cytotoxicity was also found in β-ELE treated cells transfected with $TFEB^{S122D}$, $TFEB^{S211D}$, and $TFEB^{S122D, S211D}$ (Fig. S7A). These results indicated that TFEB positively related to β-ELE induced ferroptosis. To further confirm this phenomenon, we overexpress TFEB in β-ELE treated A549 cells. β-ELE induced cytotoxicity and lipid ROS was obviously promoted by the overexpression of TFEB (Fig. 6C&D), as well as the decline on the expression of SLC7A11 and GPX4 (Fig. 6E&S7B), which indicated that TFEB overexpression enhanced β-ELE induced ferroptosis.

The reduction of GPX4 can trigger ferroptosis. In order to observe whether β-ELE induced ferroptosis can be triggered directly by GPX4, we genetically changed the level of GPX4 in A549, then applied β-ELE. Knockdown of GPX4 significantly increased lipid ROS in A549, while the increasement was further promoted in $A549^{TFEB\ KO}$ cells (Fig. 6B), which might be due to the relative high level of GPX4 in $A549^{TFEB\ KO}$ cells and the reduction of GPX4 is much more robustly. Meantime, as the GPX4 basal level is lower in GPX4 knockdown A549 cells, β-ELE induced GPX4 decrease is much less compared with that in wide type A549 cells, which might be contribute to the slight increase on β-ELE induced lipid ROS in GPX4 knockdown A549 cells (Fig. 6B). β-ELE induced lipid ROS increasement abolished in GPX4 knockdown $A549^{TFEB\ KO}$ cells, but not in GPX4 knockdown A549 cells (Fig. 6B), which indicated that β-ELE induced lipid ROS increasement is dependent on TFEB, but not directly targeted on GPX4.

Next, we observed the role of GPX4 in TFEB mediated ferroptosis in β-ELE treated NSCLC cells, TFEB overexpression promoted β-ELE induced lipid ROS formation, which attenuated by the overexpression of GPX4 (Fig. 6D). Intriguingly, the overexpress of GPX4 itself can also compromise the lipid ROS formation induced by β-ELE, which is more obvious than that in β-ELE treated NSCLC cells

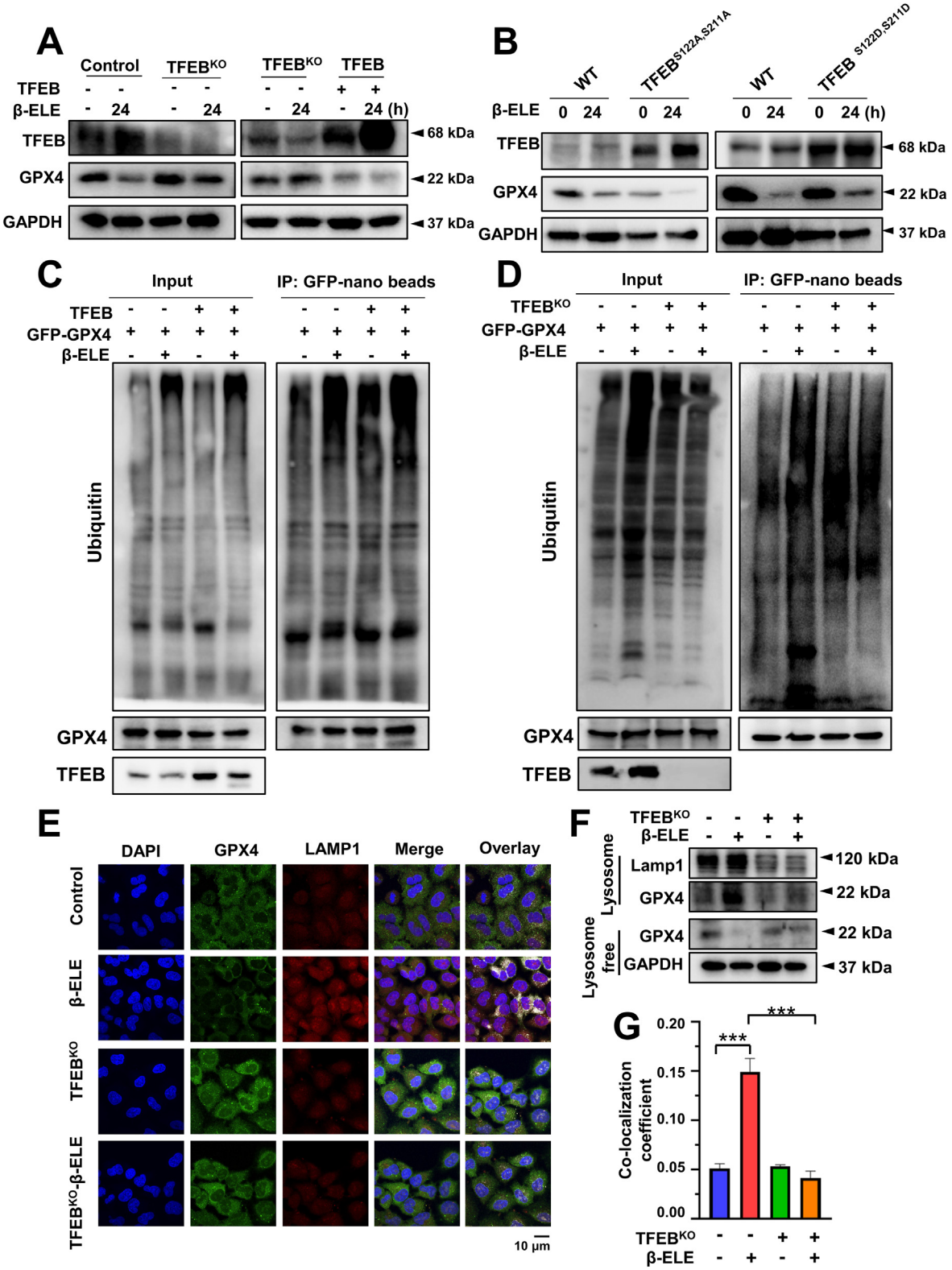

Fig. 4. TFEB promotes GPX4 degradation in β-ELE treated NSCLC. (A) A549 and A549$^{TFEB\ KO}$ cells were transfected with or without TFEB (10 μg/10 cm dish) plasmid for 24 h, then treated with β-ELE (120 μg/mL) for 24 h. The protein level of TFEB and GPX4 were detected by western blot. (B) A549 cells transfected with or without TFEB$^{S122A,\ S211A}$ (10 μg/10 cm dish), TFEB$^{S122D,\ S211D}$ (10 μg/10 cm dish), then treated with β-ELE (120 μg/mL) for 24 h. S122A and S211A are dephosphorylation-mimicking mutations of TFEB, while S122D and S211D are phosphorylation-mimicking mutations of TFEB. The protein level of TFEB and GPX4 were detected by western blot. (C, D) A549 cells were co-transfected with GPX4-GFP (10 μg/10 cm dish) and TFEB (10 μg/10 cm dish) (C), A549 and A549$^{TFEB\ KO}$ cells were transfected with GPX4-GFP (10 μg/10 cm dish) (D), then treated with β-ELE for 24 h. Cells were lysed with RIPA buffer, cell lysates were then subjected to IP via GFP-nanobeads and analyzed by western blot with antibodies as indicated (TFEB, GPX4). (E) A549 and A549$^{TFEB\ KO}$ cells were treated with β-ELE (120 μg/mL) for 24 h, the co-localization of GPX4 and LAMP1 was detected by immunofluorescence. Bar = 10 μm. (F) A549 cells and A549$^{TFEB\ KO}$ cells were treated with or without β-ELE (120 μg/mL) for 24 h. Lysosomes and lysosome-free cell lysates were collected and the protein level of GPX4 was measured by western blot. LAMP1 and GAPDH were used as loading controls of lysosomal and non-lysosomal fractions respectively. (G) Co-localization coefficients from (E) were calculated by Olympus Fluoview FV31S-DT Software. Each point represents the mean ± SEM. $n = 3$, $^{***}P < 0.001$.

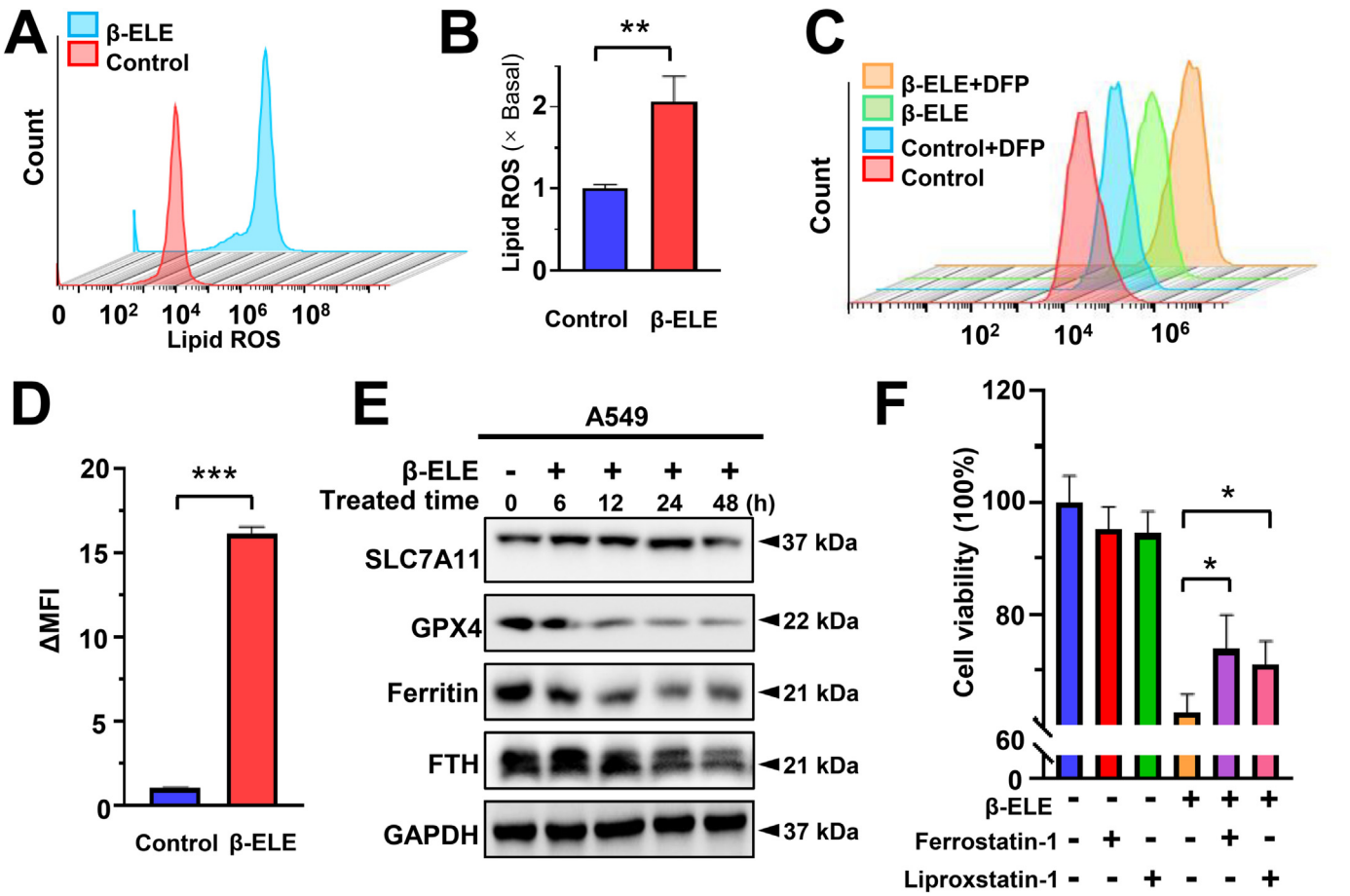

Fig. 5. β-ELE induces ferroptosis in A549 cells. (A) A549 cells were treated with β-ELE (120 μg/mL) for 24 h, and stained with BODIPY™ 581/591 C11 (10 μM) for 30 min. Upon oxidation, its excitation maximum shifts from 581 to 500 nm and the emission maximum shifts from 591 to 510 nm. The level of lipid peroxidation was detected by flow cytometry. (B) The level of lipid peroxidation from (A) was calculated by FlowJo. (C) A549 cells were treated with β-ELE for 24 h, CA-AM was added to cells at the final concentration of 0.5 μM, followed by adding iron chelator deferiprone (DFP, 100 μM) for 1 h or left untreated. The mean fluorescence was detected fluorescence microplate reader (Exc = 488 nm, Em = 525 nm). (D) The amount of LIP was reflected via difference on mean fluorescence of each sample with or without deferiprone from (C). (E) A549 cells were treated with β-ELE for 6, 12, 24 and 48 h, the protein level of SLC7A11, GPX4, Ferritin and FTH were detected by western blot. GAPDH was used as a loading control. (F) A549 cells were treated with β-ELE after 1 h in the presence or absence of ferroptosis inhibitors Ferrostatin-1 (2 μM) or Liproxstatin-1 (50 nM). Cell viability was detected by MTT assay. Each point represents the mean ± SEM. $n = 3$, $^{*}P < 0.05$, $^{**}P < 0.01$, $^{***}P < 0.001$.

with GPX4 and TFEB co-overexpression (Fig. 6D). This might be due to the high level of TFEB contributed to the decline of GPX4, β-ELE induced GPX4 decline in NSCLC cells with GPX4 and TFEB co-overexpression is not as obvious as that in cells with GPX4 single overexpression. All these data indicated that GPX4 decline is required for TFEB mediated ferroptosis in β-ELE treated A549 cells.

Meantime, TFEB promoted β-ELE induced increase on lysosome activity, characterized by the increase on the mean fluorescence of LysoTracker stained cells (Fig. 6F). And the blockage of lysosome activity compromised the anticancer effect of β-ELE (Fig. S7C). All these indicated that TFEB promoted β-ELE induced ferroptosis in NSCLC, which also positively related to lysosome activity.

Knockout of TFEB attenuates anticancer effect of β-ELE in orthotopic NSCLC NOD/SCID mouse model

To confirm the role of TFEB on β-ELE induced anticancer effect, we evaluated the anticancer effect of β-ELE in orthotopic NOD/SCID mouse model established with A549-luci or A549$^{TFEB\ KO}$-luci cells. Tumor growth was monitored by bioluminescence each week after administration. The bioluminescence has no significant change between groups at day 1. Subsequent increase in bioluminescence was detected in A549-luci and A549$^{TFEB\ KO}$-luci control groups, indicating the rapid tumor growth. β-ELE significantly inhibited the tumor growth since day 7, characterized by the sharply decrease in bioluminescence. The inhibitory effect was most obvious on day 21, the bioluminescence reduced more than 50% compared with A549-luci group. However, in A549$^{TFEB\ KO}$-luci mice, the anticancer effect of β-ELE was not as strong as that in A549-luci mice, which indicated that TFEB knockout compromised β-ELE induced anticancer effect in vivo (Fig. 7A&B).

To observe the change of GPX4 distribution after TFEB knockout in vivo, immunohistofluorescence was applied to observed the co-localization of LAMP1 and GPX4 in tumor of murine lung tissues. Consisting with the in vitro data, TFEB knockout attenuated β-ELE induced increase on the co-localization of LAMP1 and GPX4, which indicated TFEB contribute to β-ELE induced GPX4 lysosome distribution and GPX4 decline (Fig. 7C&D). To further confirm the function of TFEB in the β-ELE induced anticancer effect, the expression level of PCNA in the tumors was detected by immunohistochemistry. PCNA is a nuclear non-histone protein that is necessary for DNA synthesis, thus higher expression levels are noted during G1-S phase transition. The expression levels of PCNA were high in A549-luci and A549$^{TFEB\ KO}$-luci control groups (Fig. 7E&F), while the expression of PCNA were lower in β-ELE treated groups. Under β-ELE treatment, the expression of PCNA in the A549-luci mice was reduced approximately 49% compared with that in the A549$^{TFEB\ KO}$-luci mice, which indicated that β-ELE

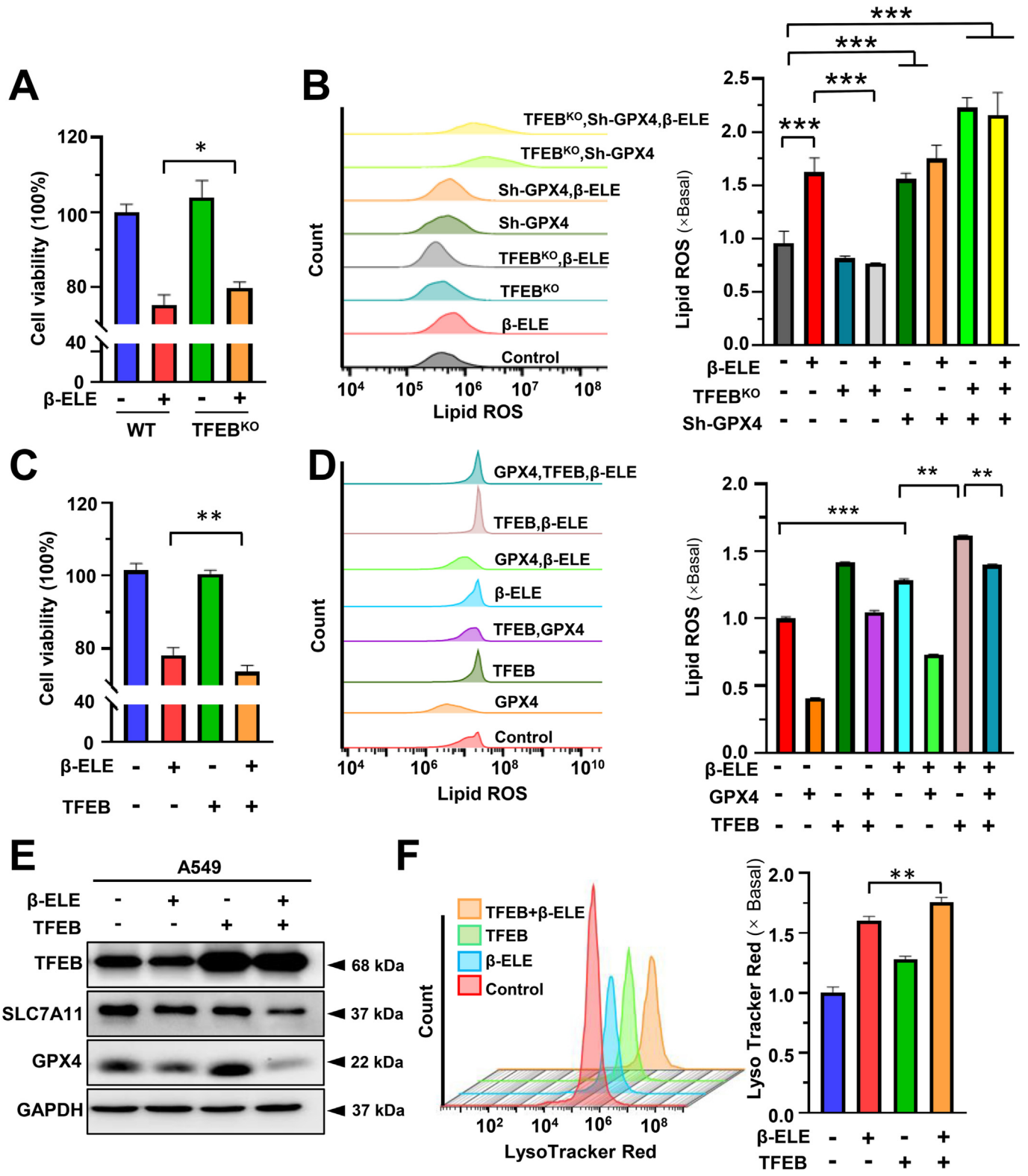

Fig. 6. TFEB promotes β-ELE induced ferroptosis in NSCLC. (A) β-ELE (120 μg/mL) was applied to A549 and A549$^{TFEB\ KO}$ cells for 24 h, the proliferation inhibition of the cells was detected by MTT assay. (B) A549 and A549$^{TFEB\ KO}$ cells were transfected with Sh-GPX4 (constructed in psi-LVRU6MP vector with mCherry, Gene ID = 2879, HSH118768-LVRU6MP, GeneCopoeia) for 8 h, then removed medium and treated with β-ELE (120 μg/mL) for 24 h. Cells were stained with BODIPY™ 581/591 C11 (10 μM) for 30 min. After washed cells with three times of PBS, cells were resuspended in PBS at the density of 0.5 × 10^6 cells/mL, the level of lipid peroxidation was detected by flow cytometry. (C) A549 cells were transfected with vector (pcDNA3.1) or TFEB, then treated β-ELE (120 μg/mL) for 24 h, the inhibition on proliferation was detected by MTT assay. (D) A549 cells were transfected with TFEB or GPX4, or co-transfected with GPX4 and TFEB, then treated with β-ELE (120 μg/mL) for 24 h, and the process of detecting lipid peroxidation is the same as that in (B). (E) A549 cells were transfected with vector (pcDNA3.1) or TFEB, then treated with β-ELE (120 μg/mL) for 24 h, the protein level of TFEB, SLC7A11 and GPX4 were detected by western blot. GAPDH was used as a loading control. (F) The transfection and drug treatment were same as in (E). The fluorescent signals were detected by flow cytometry after staining with LysoTracker Red (50 nM) for 30 min. Each point represents the mean ± SEM.n = 3, $^*P < 0.05$, $^{**}P < 0.01$, $^{***}P < 0.001$.

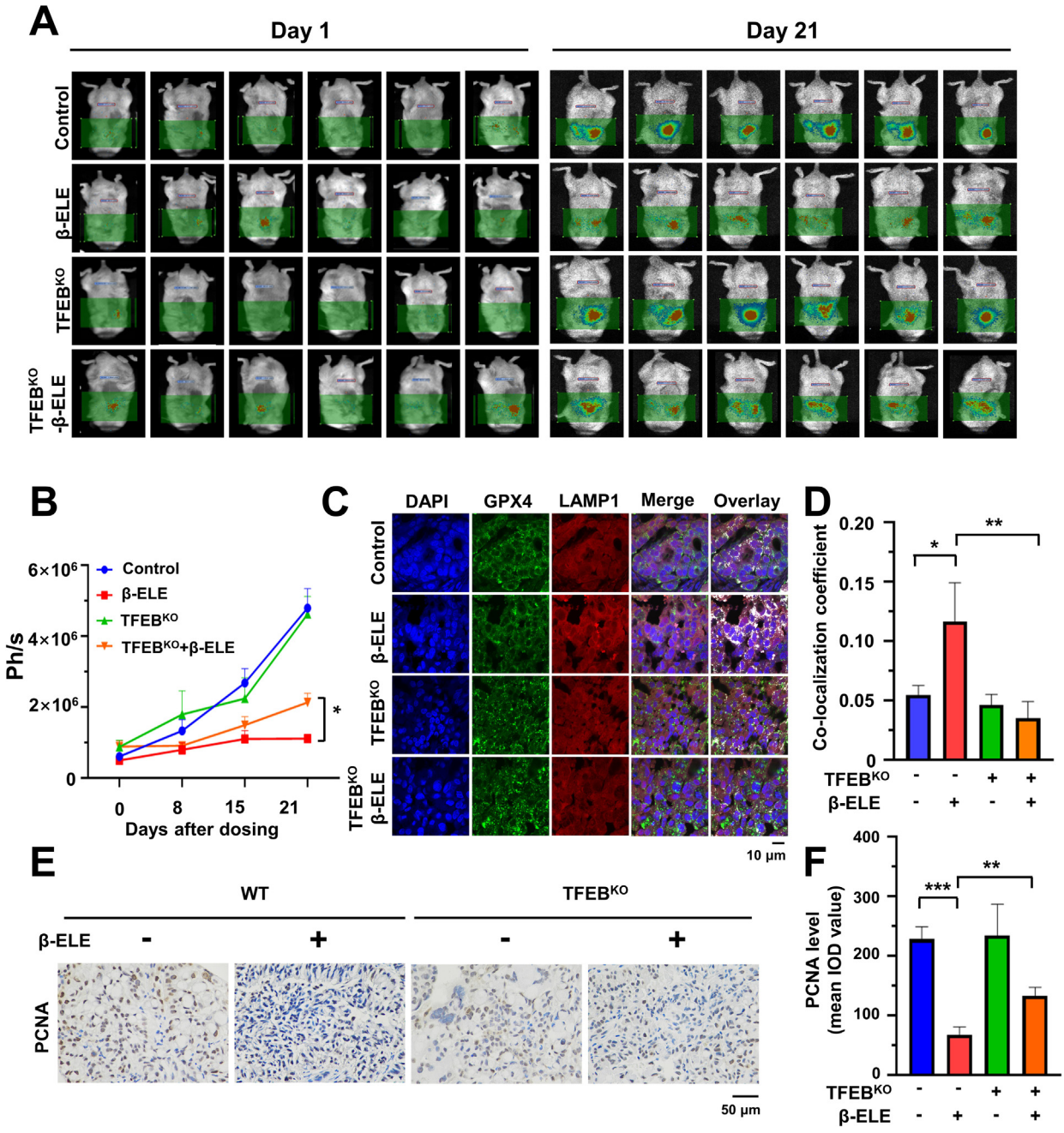

Fig. 7. Knock out of TFEB attenuates anticancer effect of β-ELE in orthotopic NSCLC NOD/SCID mouse model. Male NOD/SCID mice aged 4–5 weeks old were used in the study. A549-luci or A549$^{TFEB\ KO}$-luci cells (1×10^6 in 100 μL 0.9% normal saline) were injected into the right lung of each mouse. After five days later, the mice were divided into 4 groups (6 mice pre group) and administered with β-ELE (120 mg/kg) by tail vein injection. On day 21 after administration, mice were sacrificed and tumor tissue samples were frozen in -80 °C or fixed in 4% PFA for IF or IHC respectively. The experiment was performed as described in materials and methods. (A) Representative images of bioluminescence at indicated time points (Day1, Day21) after β-ELE administration. (B) Bioluminescence intensity of mice. The signals are expressed in radiance (Ph/s). $n = 6$. (C) Co-localization of GPX4 and LAMP1 in tumor was detected by immunofluorescence. Bar = 10 μm. (D) Co-localization coefficients from (C) were calculated by Olympus Fluoview FV31S-DT Software. $n = 4$. (E) Immunohistochemical staining analysis. PCNA positive cells in the sections are stained brown. The nuclei are stained blue. Representative figures from each group are shown. (F) Each tumor tissue section was randomly selected for the calculation of the mean IOD value of the positive region through Image Pro Plus software, which indicated the amount of PCNA expression. Bar = 50 μm. Each point represents the mean ± SEM. $n = 6$. $^*P < 0.05$, $^{**}P < 0.01$, $^{***}P < 0.001$.

induced inhibition on PCNA could be compromised by TFEB knockout (Fig. 7E&F). All these data indicated that TFEB promoted GPX4 lysosome localization and anticancer effect induced by β-ELE.

Discussion

Multiple researches demonstrated the anti-lung cancer effect of β-ELE. However, the potential target for its anti-lung cancer effect is still not clear, and the studies on target protein of β-ELE based on protein-ligand binding experiments are seldom. Emerging evidences indicated that TFEB is the potential target for cancer therapy. However, the reported dual function of TFEB on cancer biology made it still unclear how it affect cancer development in lung cancer. TFEB is the master regulator of autophagy, lysosome biogenesis, TAM, etc, its role on ferroptosis, a promising strategy for cancer therapy, is still in its infancy. As the mechanisms of natural anticancer agents are usually diverse and not fully understood,

using natural anticancer agents with the function of TFEB activation and ferroptosis induction may help us to understand the novel biological event during TFEB-mediated regulation on ferroptosis. Here, we found β-ELE has binding affinity to TFEB, and molecular docking reveals the binding sites might be located at ZIP region, which is crucial for TFEB activation. β-ELE can both trigger TFEB activation and ferroptosis in EGFR wild-type NSCLC. The role of TFEB in β-ELE treated ferroptosis are illustrated in vitro and in vivo by several folds: (i) TFEB positively related to β-ELE induced ferroptosis; (ii) TFEB negatively related to the protein expression of ferroptosis negative regulator GPX4; (iii) TFEB knockout compromised GPX4 lysosome translocation and degradation. (iv) The anti-lung cancer effect of β-ELE was compromised by TFEB knockout in vivo.

Targeting TFEB is a promising therapeutic approach for cancer treatment. In the past, majority of studies revealed the positive relationship of TFEB with cancer development, however, with the new discovery of the function of TFEB in various cancer biological events, the negative role of TFEB in cancer development has been reported in recent studies [36–38]. Activation of TFEB can suppress cancer cell metastasis and proliferation via TAM, TEM, EMT and lysosome degradation [36,39,40]. In NSCLC, low level of TFEB in tumor tissues are associated with poor prognosis in patients [41]. Thus, pharmacological activation of TFEB showed benefit for cancer therapy. In this study, we found that β-ELE can bind and activate TFEB, and the TFEB knockout compromised the anticancer effect of β-ELE both in vitro and in vivo, which indicated its negative role on tumor progression in NSCLC.

The regulation of TFEB on NSCLC mainly depends on lysosome activity. Several studies showed that the anticancer agents induce ferroptosis via TFEB-mediated lysosomal activation [42,43] Ferroptosis is a type of programmed cell death, characterized by the elevation on iron and lipid oxidation. Ferroptosis evasion can lead to tumor progression and therapeutic resistance [10]. Cancer cell has high load of ROS and iron addiction, which render them susceptible to ferroptosis [12]. As the apoptosis resistance is the key shortage for cancer treatment, targeting lysosome and ferroptosis is the promising approach to improve anticancer effect. Several studies reported that β-ELE can induce apoptosis in very high concentration, however, in our previous study, apoptosis marker was not obviously changed at the concentration of 120 μg/ml, as well as the key protein of autophagy (Fig. S8A). While the ferroptosis induction was much obvious. Considering β-ELE induced ferroptosis concomitant with TFEB and lysosome activation, TFEB mediated lysosome activation might be the key process for ferroptosis induction. The mechanism on TFEB-mediated ferroptosis is not yet fully understood. One study indicated that TFEB promoted lysosome degradation of ferritin, a negative regulator of ferroptosis, finally triggered ferroptosis [19]. However, the regulation of TFEB on negative key regulator of ferroptosis, GPX4, is not elucidated. In our study, the most changeable ferroptosis regulator during β-ELE induced ferroptosis was GPX4. Thus, TFEB might promote GPX4 degradation to trigger ferroptosis.

GPX4 is the key negative regulator for ferroptosis, as the induction of ferroptosis would directly or indirectly suppress GPX4. Recent studies indicated that the enhanced level and activity of GPX4 is positively related to tumorigenesis [10]. GPX4 inhibition is an effective way to trigger ferroptosis. It was reported that GPX4 can be degraded by chaperone mediated autophagy (CMA), which finally degraded GPX4 in lysosome. However, the role of TFEB in CMA mediated autophagy is not fully elucidated. Considering TFEB is the master regulation of lysosome biogenesis, We hypothesis that TFEB activation can directly promote the GPX4 lysosome degradation. The lysosome degradation needs ubiquitination of target proteins, although it was reported that both K63 and K48 polyubiquitination involved in this process, majority studies showed that K63 polyubiquitination chain mainly involved in lysosome degradation [44,45]. Here, we found that GPX4 sharply declined in β-ELE treated NSCLC cells, which is not due to the transcriptional change but the enhanced lysosome degradation, and the polyubiquitination chain of GPX4 is mainly K63 linked (Fig. S8B). TFEB knockout reduced β-ELE induced ubiquitination of GPX4, and its translocation to lysosome, finally reversed the decline of GPX4. These phenomena indicated that TFEB positively related to GPX4 lysosome degradation in β-ELE treated EGFR wide-type NSCLC cells.

In this study, we discovered TFEB is a potential target of β-ELE in treating EGFR wide-type NSCLC cells. As TFEB is highly expressed in lung cancer, and the reported studies demonstrated the negative role of TFEB in lung cancer progression, this strategy seems promising to clinical usage. In addition, the direct evidence of TFEB promoted GPX4 lysosome degradation has not been reported. This is first time to reveal this phenomenon in natural anti-cancer agent β-ELE treated NSCLC cells, which will give a clue on NSCLC treatment strategy development and natural anticancer agents screening. However, how β-ELE bind to the ZIP region of TFEB, and why K63 poly ubiquitination is dominant in this post-translational modification are still need to be further studied.

Conclusion

Although the anti-lung cancer activity of β-ELE was discovered a decade ago, the therapeutic target and mechanism are still not clear. The reported studies mainly focus on efficacy studies and the impact on some oncogenic pathways. However, the special binding protein of β-ELE based on "gold" standard measurement for protein-ligand binding, e.g. SPR, has not yet been reported. Furthermore, the mechanical studies are mainly focus on reported signaling pathway involved in lung cancer development, the mechanical studies on lysosome degradation are seldom.

The natural compound usually has some unknow anticancer mechanism responsible for their anticancer activity. In this study, we use β-ELE to unveiling the unique anticancer mechanism, which might give a glue to develop a novel approach to address NSCLC. First, protein-ligand binding experiment SRP was firstly used to demonstrate that β-ELE has binding affinity to TFEB. Second, the first time to reveal that TFEB promoted β-ELE induced ferroptosis and anticancer effect in NSCLC, knockout of TFEB attenuated β-ELE induced ferroptosis and anticancer effect in orthotopic NSCLC NOD/SCID mouse model. Third, as the upstream effect of TFEB on GPX4 has not yet be elucidated, the observation on the biological events during β-ELE mediated anticancer process help to reveal a novel process that TFEB increase GPX4 lysosome degradation and consequent event ferroptosis, which could be a novel strategy for NSCLC therapy.

Practical application

This study discovered that lysosomal master regulator TFEB mediated GPX4 degradation could be a potential novel mechanism for TFEB-mediated ferroptosis in β-ELE treated NSCLC cells. As cancer cells can evade apoptosis, targeting lysosome and ferroptosis are promising strategy for anticancer. The novel mechanism illustrated in this study will broaden the use of β-ELE as a lysosome targeting anticancer agent. Furthermore, the TFEB-mediated lysosome degradation of GPX4 could be developed to be a promising approach for ferroptosis induction.

Declaration of Competing Interest

The authors declare that they have no known competing financial interests or personal relationships that could have appeared to influence the work reported in this paper.

Acknowledgments

This work is supported by the National Natural Science Foundation of China [82174024]; the Natural Science Foundation of Zhejiang Province [LY20H280011]; and the Medical Health Science and Technology Project of Zhejiang Provincial Health Commission [2020RC103, 2022KY1054].

Appendix A. Supplementary data

Supplementary data to this article can be found online at https://doi.org/10.1016/j.jare.2023.08.018.

References

[1] Xia C, Dong X, Li H, Cao M, Sun D, He S, et al. Cancer statistics in China and United States, 2022: profiles, trends, and determinants. Chin Med J (Engl) 2022;135:584–90. doi: https://doi.org/10.1097/CM9.0000000000002108.
[2] Yang Y, Li N, Wang TM, Di L. Natural products with activity against lung cancer: A review focusing on the tumor microenvironment. Int J Mol Sci 2021;22:10827. doi: https://doi.org/10.3390/ijms221910827.
[3] Zhong L, Li Y, Xiong L, Wang W, Wu M, Yuan T, et al. Small molecules in targeted cancer therapy: advances, challenges, and future perspectives. Signal Transduct Target Ther 2021;6:201. doi: https://doi.org/10.1038/s41392-021-00572-w.
[4] Yuan M, Huang LL, Chen JH, Wu J, Xu Q. The emerging treatment landscape of targeted therapy in non-small-cell lung cancer. Signal Transduct Target Ther 2022;4:61. doi: https://doi.org/10.1038/s41392-019-0099-9.
[5] Tabchi S, Kourie HR, Klastersky J. Concurrent driver mutations/rearrangements in non-small-cell lung cancer. Curr Opin Oncol 2017;29:118–22. doi: https://doi.org/10.1097/CCO.0000000000000353.
[6] Wen T, Song L, Hua S. Perspectives and controversies regarding the use of natural products for the treatment of lung cancer. Cancer Med 2021;10:2396–422. doi: https://doi.org/10.1002/cam4.3660. Epub 2021 Mar 2.
[7] Shah R, Lester JF. Tyrosine kinase inhibitors for the treatment of EGFR mutation-positive non–small-cell lung cancer: A clash of the generations. Clin Lung Cancer 2020;21:e216–28. doi: https://doi.org/10.1016/j.cllc.2019.12.003.
[8] Galluzzi L, Vitale I, Aaronson SA, Abrams JM, Adam D, Agostinis P, et al. Molecular mechanisms of cell death: recommendations of the Nomenclature Committee on Cell Death 2018. Cell Death Differ 2018;25:486–541. doi: https://doi.org/10.1038/s41418-017-0012-4.
[9] Mou Y, Wang J, Wu J, He D, Zhang C, Duan C, et al. Ferroptosis, a new form of cell death: opportunities and challenges in cancer. J Hematol Oncol 2019;12:34. doi: https://doi.org/10.1186/s13045-019-0720-y.
[10] Stockwell BR. Ferroptosis turns 10: Emerging mechanisms, physiological functions, and therapeutic applications. Cell 2022;185:2401–21. doi: https://doi.org/10.1016/j.cell.2022.06.003.
[11] Lei G, Zhuang L, Gan B. Targeting ferroptosis as a vulnerability in cancer. Nat Rev Cancer 2022;22:381–96. doi: https://doi.org/10.1038/s41568-022-00459-0.
[12] Rodriguez R, Schreiber SL, Conrad M. Persister cancer cells: Iron addiction and vulnerability to ferroptosis. Mol Cell 2022;82:728–40. doi: https://doi.org/10.1016/j.molcel.2021.12.001.
[13] Seibt TM, Proneth B, Conrad M. Role of GPX4 in ferroptosis and its pharmacological implication. Free Radic Biol Med 2019;133:144–52. doi: https://doi.org/10.1016/j.freeradbiomed.2018.09.014.
[14] Feng H, Stockwell BR. Unsolved mysteries: How does lipid peroxidation cause ferroptosis? PLoS Biol 2018;16(5):e2006203.
[15] Yang WS, SriRamaratnam R, Welsch ME, Shimada K, Skouta R, Viswanathan VS, et al. Regulation of ferroptotic cancer cell death by GPX. Cell 2014;156:317–31. doi: https://doi.org/10.1016/j.cell.2013.12.010.
[16] Akimov V, Barrio-Hernandez I, Hansen SVF, Hallenborg P, Pedersen AK, Bekker-Jensen DB, et al. UbiSite approach for comprehensive mapping of lysine and N-terminal ubiquitination sites. Nat Struct Mol Biol 2018;25:631–40. doi: https://doi.org/10.1038/s41594-018-0084-y.
[17] Yang L, Chen X, Yang Q, Chen J, Huang Q, Yao L, et al. Broad spectrum deubiquitinase inhibition both apoptosis and ferroptosis in cancer cells. Front Oncol 2020;10:949. doi: https://doi.org/10.3389/fonc.2020.00949.
[18] Huang F, Zeng X, Kim W, Balasubramani M, Fortian A, Gygi SP, et al. Lysine 63-linked polyubiquitination is required for EGF receptor degradation. Proc Natl Acad Sci U S A 2013;110:15722–7. doi: https://doi.org/10.1073/pnas.1308014110.
[19] An S, Hu M. Quercetin promotes TFEB nuclear translocation and activates lysosomal degradation of ferritin to induce ferroptosis in breast cancer cells. Comput Intell Neurosci 2022;2022:5299218. doi: https://doi.org/10.1155/2022/5299218.
[20] Wu Z, Geng Y, Lu X, Shi Y, Wu G, Zhang M, et al. Chaperone-mediated autophagy is involved in the execution of ferroptosis. Proc Natl Acad Sci U S A 2019;116:2996–3005. doi: https://doi.org/10.1073/pnas.1819728116.
[21] Yu S, Li Z, Zhang Q, Wang R, Zhao Z, Ding W, et al. GPX4 degradation via chaperone-mediated autophagy contributes to antimony-triggered neuronal ferroptosis. Ecotoxicol Environ Saf 2022;234:. doi: https://doi.org/10.1016/j.ecoenv.2022.113413113413.
[22] Lou JS, Zhao LP, Huang ZH, Chen XY, Xu JT, Tai WCS, et al. Ginkgetin derived from Ginkgo biloba leaves enhances the therapeutic effect of cisplatin via ferroptosis-mediated disruption of the Nrf2/HO-1 axis in EGFR wild-type non-small-cell lung cancer. Phytomedicine 2021;80:. doi: https://doi.org/10.1016/j.phymed.2020.153370153370.
[23] Tang J, Ren YG, Zhao J, Long F, Chen JY, Jiang Z. Shikonin enhances sensitization of gefitinib against wild-type EGFR non-small cell lung cancer via inhibition PKM2/stat3/cyclinD1 signal pathway. Life Sci 2018;204:71–7. doi: https://doi.org/10.1016/j.lfs.2018.05.012.
[24] Han SY, Ding HR, Zhao W, Teng F, Li PP. Enhancement of gefitinib-induced growth inhibition by Marsdenia tenacissima extract in non-small cell lung cancer cells expressing wild or mutant EGFR. BMC Complement Altern Med 2014;14:1–11. doi: https://doi.org/10.1186/1472-6882-14-165.
[25] Sun L, Yim WS, Fahey P, Wang S, Zhu X, Qiao J, et al. Investigation on advanced non-small-cell lung cancer among elderly patients treated with Chinese herbal medicine versus chemotherapy: a pooled analysis of individual data. Evid Based Complement Alternat Med 2019;2019. doi: https://doi.org/10.1155/2019/1898345.
[26] Zhai B, Zeng Y, Zeng Z, Zhang N, Li C, Zeng Y. Drug delivery systems for elemene, its main active ingredient β-elemene, and its derivatives in cancer therapy. Int J Nanomedicine 2018;13:6279–96. doi: https://doi.org/10.2147/IJN.S174527.
[27] Cai H, Ren L, Wang Y, Zhang Y. Beta-Elemene reduces the malignancy of non-small cell lung cancer by enhancing C3orf21 expression. Front Oncol 2021;11:. doi: https://doi.org/10.2147/IJN.S174527571476.
[28] Zhang H, Li S, Bao J, Ge N, Hong F, Qian L. β-elemene inhibits non-small cell lung cancer cell migration and invasion by inactivating the FAK-Src pathway. Exp Ther Med 2021;22:1095. doi: https://doi.org/10.3892/etm.2021.10529.
[29] Zheng F, Tang Q, Zheng XH, Wu J, Huang H, Zhang H, et al. Inactivation of Stat3 and crosstalk of miRNA155-5p and FOXO3a contribute to the induction of IGFBP1 expression by beta-elemene in human lung cancer. Exp Mol Med 2018;50:1–14. doi: https://doi.org/10.1038/s12276-018-0146-6.
[30] Shi F, Yang G, Ren J, Guo T, Du Y, Feng N. Formulation design, preparation, and in vitro and in vivo characterizations of β-Elemene-loaded nanostructured lipid carriers. Int J Nanomedicine 2013;8:2533–41. doi: https://doi.org/10.2147/IJN.S46578.
[31] Wang Y, Deng Y, Mao S, Jin S, Wang J, Bi D. Characterization and body distribution of beta-elemene solid lipid nanoparticles (SLN). Drug Dev Ind Pharm 2005;31:769–78. doi: https://doi.org/10.1080/03639040500216329.
[32] Chen W, Li Y, Liu C, Kang Y, Qin D, Chen S, et al. In situ engineering of tumor-associated macrophages via a nanodrug-delivering-drug (β-Elemene @Stanene) strategy for enhanced cancer chemo-immunotherapy. Angew Chem Int Ed Engl 2023:e202308413.
[33] Huang M, Lu JJ, Ding J. Natural products in cancer therapy: Past. Present and Future Nat Prod Bioprospect 2021;11:5–13. doi: https://doi.org/10.1007/s13659-020-00293-7.
[34] Gong Z, Liu ZG, Du KY, Wu JH, Yang N, Malhotra A, et al. Potential of β-elemene induced ferroptosis through Pole2-mediated p53 and PI3K/AKT signaling in lung cancer cells. Chem Biol Interact 2022;365:. doi: https://doi.org/10.1016/j.cbi.2022.110088110088.
[35] Xu C, Jiang ZB, Shao L, Zhao ZM, Fan XX, Sui X, et al. β-Elemene enhances erlotinib sensitivity through induction of ferroptosis by upregulating lncRNA H19 in EGFR-mutant non-small cell lung cancer. Pharmacol Res 2023;191. doi: https://doi.org/10.1016/j.phrs.2023.106739.
[36] Li Y, Hodge J, Liu Q, Wang J, Wang Y, Evans TD, et al. TFEB is a master regulator of tumor-associated macrophages in breast cancer. J Immunother Cancer 2020;8:e000543.
[37] Zhang C, Yang H, Pan L, Zhao G, Zhang R, Zhang T, et al. Hepatites B virus X protein (HBx) suppresses transcription factor EB (TFEB) resulting in stabilization of integrin Beta 1 (ITGB1) in hepatocellular carcinoma cells. Cancers (Basel) 2021;13:1181. doi: https://doi.org/10.3390/cancers13051181.
[38] Li S, Song Y, Quach C, Guo H, Jang GB, Maazi H, et al. Transcriptional regulation of autophagy-lysosomal function in BRAF-driven melanoma progression and chemoresistance. Nat Commun 2019;10:1693. doi: https://doi.org/10.1038/s41467-019-09634-8.
[39] Fang L, Hodge J, Saaoud F, Wang J, Iwanowycz S, Wang Y, et al. Transcriptional factor EB regulates macrophage polarization in the tumor microenvironment. Oncoimmunology 2017;6:e1312042.
[40] Liu N, Luo J, Kuang D, Xu S, Duan Y, Xia Y, et al. Lactate inhibits ATP6V0d2 expression in tumor-associated macrophages to promote HIF-2α-mediated tumor progression. J Clin Invest 2019;129:631–46. doi: https://doi.org/10.1172/JCI123027.
[41] Wang L, Xu P, Xie X, Hu F, Jiang L, Hu R, et al. Down regulation of SIRT2 reduced ASS induced NSCLC apoptosis through the release of autophagy components

vis exsomes. Front Cell Dev Biol 2020;8:. doi: https://doi.org/10.3389/fcell.2020.601953601953.
[42] Krishan S, Sahni S, Richardson DR. The anti-tumor agent, Dp44mT, promotes nuclear translocation of TFEB via inhibition of the AMPK-mTORC1 axis. Biochim Biophys Acta Mol Basis Dis 2020;1866:. doi: https://doi.org/10.1016/j.bbadis165970.
[43] Zhang X, Guo Y, Li H, Han L. FIN56, a novel ferroptosis inducer, triggers lysosomal membrane permeabilization in a TFEB-dependent manner in glioblastoma. J Cancer 2021;12:6610–9. doi: https://doi.org/10.7150/jca.58500.
[44] Zhang L, Xu M, Scotti E, Chen Z, Tontonoz P. Both K63 and K48 ubiquitin linkages signal lysosomal degradation of the LDL receptor. J Lipid Res 2013;54:1410–20. doi: https://doi.org/10.1194/jlr.M035774.
[45] Zhao L, Zhao J, Zhong K, Tong A, Jia D. Targetd protein degradation: mechanisms, strategies and application. Signal Transduct Target Ther 2022;7:113. doi: https://doi.org/10.1038/s41392-022-00966-4.